https://doi.org/10.5194/acp-2022-653
Preprint. Discussion started: 11 October 2022

Atmospheric Chemistry and Physics Discussions

Determination of the chemical equator from GEOS-Chem model simulation: a focus on the Tropical Western Pacific region

Xiaoyu Sun[1], Mathias Palm[1], Justus Notholt[1], and Katrin Müller[2]

[1]Institute of Environmental Physics, University of Bremen, Otto-Hahn-Allee 1, 28359 Bremen, Germany
[2]Alfred Wegener Institute, Helmholtz Centre for Polar and Marine Research, Telegrafenberg A43, 14473 Potsdam, Germany

Correspondence: Xiaoyu Sun (xiaoyu_sun@iup.physik.uni-bremen.com)

Abstract. The Tropical Western Pacific (TWP) plays an important role for global stratosphere-troposphere exchange and is an active region of interhemispheric transport. Common indicators for transport between the hemispheres like the tropical rain belt are too broad or lack precision in the TWP. In this paper, we provide a method to determine the atmospheric chemical equator (CE), which is a boundary for air mass transport between the two hemispheres in the tropics. This method used the model output from an artificial passive tracer simulated by the chemical transport model GEOS-Chem in the troposphere. We investigated the movement of the CE in the tropics, which indicates the migration of atmospheric circulation systems and air mass origins. Our results show the CE in different time scales suggesting that the different features of the interhemispheric transport in different regions are highly related to the variation of the circulation systems. We compared the CE with the tropical wind fields, indicating that the region of interhemispheric transport does not coincide with the convergence of the 10 m wind fields, in the tropical land sectors and the TWP region. We discussed the vertical extent and the meridional extent of the interhemispheric transport. We found that the vertical structure had a slight northern tilt in the boreal winter season and a southern tilt in summer, meaning the speed of the migration of the CE decreases with the altitude. The meridional extent of the CE indicates a narrow transition zone where interhemispheric transport happens throughout the year. We found that the meridional extent above South America is larger compared to other regions. The distribution of the land-sea contrast plays an important role in the meridional extent of interhemispheric transport. We focused on the TWP region and further compared the tropical rain belt with the CE. There is a broad region of high precipitation which determines the region of the interhemispheric transport. In the NH winter, the CE are not consistent with the tropical rain belt in TWP, which lies to the southern branch of the peak of the rain belt. For the other season, the daily CE showed agreement with the peak of the tropical rain belt in the TWP region.

1 Introduction

The Tropical West Pacific Region (TWP) is an area extending from the Maritime Continent (Ramage, 1968) to the International Date Line, with some of the world's highest sea surface temperatures. The TWP warm pool provides the environment in which deep convective cloud systems develop (Fueglistaler et al., 2004). The tropospheric air ascends into the stratosphere via the tropical tropopause layer (TTL) mainly in this region, TWP is considered as the major transport pathway from the troposphere

https://doi.org/10.5194/acp-2022-653
Preprint. Discussion started: 11 October 2022

Atmospheric Chemistry and Physics Discussions

into the stratosphere during Northern Hemispheric (NH) winter (Newell and Gould-Stewart, 1981; Fueglistaler et al., 2004; Krüger et al., 2008; Rex et al., 2014). Deep convection and large-scale ascent in this region enable boundary layer air heated by the warm ocean surface to ascend to the TTL, changing the composition of the TTL atmosphere across the tropics. The air mass origin in the TWP region needs to be studied to properly describe the chemical species entering the stratosphere via the troposphere stratosphere transport pathway above the TWP.

ITCZ (the Intertropical Convergence Zone) is conventionally defined as a lower-tropospheric convergence region circling the globe where the tropical trade winds from the Northern and Southern hemispheres meet, typically lying between approximately 15° S and 15° N (Waliser and Gautier, 1993). In the TWP, ITCZ migrates with seasons, towards the hemisphere that warms relative to the other (Schneider et al., 2014), indicating the migrations of the circulation in this region. Generally, it is recognized by fast vertical motion and heavy rainfall, which essentially acts as a meteorological barrier to cross-equatorial flow following the seasons. Previous studies identify the ITCZ as the boundary to interhemispheric mixing (Williams et al., 2002; Stehr et al., 2002). The location of the ITCZ affects weather conditions and air mass origin throughout the tropics. The time-mean or the climatology of ITCZ locations can be characterized by the zonal regions of heavy rainfall in the tropics. The day-to-day features of the ITCZ however can be quite changeable resulting from the interactions with monsoon systems and over the landmasses (Wang and Magnusdottir, 2006). The mechanisms controlling its position and rainfall intensity are not fully understood (Schneider et al., 2014).

There are some disadvantages to using ITCZ as an indicator of the equatorial circulation system. First, the ITCZ is difficult to define over the TWP region, because the Western Pacific Monsoon (WPM) (Smith et al., 2012) adds complexity to the tropical rain belt. This broad region of the tropical rain belt makes it difficult to determine the location of the ITCZ. Second, the equatorial precipitation over land is not simply a response to the surface convergence but is also influenced by local factors such as convection caused by topography, proximity to the sea, and variation of the regional humidity. The assumption that the seasonal cycle of rainfall in equatorial Africa is controlled by the seasonal excursion of the ITCZ is therefore still challenged and discussed. (Nicholson, 2009, 2018). In the TWP region, Hamilton et al. (2008) first introduced the term Chemical Equator (CE) rather than the ITCZ to represent the main atmospheric boundary between the two meteorological hemispheres (MH). They used CO as a tracer to investigate the CE and pointed out that this boundary between the MHs does not coincide with the ITCZ or the monsoon trough. Sulfur hexafluoride (SF_6) is another common tracer to constrain time scales of interhemispheric transport (IHT) (e.g., Geller et al., 1997; Waugh et al., 2013; Yang et al., 2019). It has a very long atmospheric lifetime (580 - 3200 yr) (Ravishankara et al., 1993; Morris et al., 1995; Ray et al., 2017), a large and constant growth rate during the last two decades (Rigby et al., 2010; Hall et al., 2011) and anthropogenic sources primarily over the NH. However, tracers with significant north-south gradients (such as CO and SF_6) are locally diverse and can be affected by human activities. So, to eliminate the regional dependency on human activities and the chemical processes with other species, an artificial tracer without such features is needed to investigate the IHT in the tropics.

This study aims to provide a tool to determine the boundary for air mass transport between the two MHs in the tropics, focusing on the TWP region. Here, we present model simulations from the passive tracer to determine this boundary. Following Hamilton et al. (2008), we use the term CE (Chemical Equator) to describe this boundary. This way, we avoid confusion with

https://doi.org/10.5194/acp-2022-653
Preprint. Discussion started: 11 October 2022

Atmospheric Chemistry and Physics Discussions

the tropical rain belt, indicated by the conventional ITCZ definition. To assess regional differences only caused by air mass transport, we switched off the chemistry in the model to develop an atmosphere pattern only due to the transport by the analyzed wind fields. This way, we can neglect chemical processes and regional dependency of the emissions occurring for real species like CO and SF_6. Additionally, the model approach yields a three-dimensional pattern of air mass transport, which allows investigation of the vertical structure of the CE and interhemispheric mixing processes.

In Sect. 2, the model descriptions with the simulation steps and set-ups were described. Section 2 also introduced the method of how to derive the location of CE from the simulation results. In Sect. 3, the CE location results were shown in different seasons and regions. We compared the CE locations with the tropical rain belt and wind fields from reanalysis data. We investigated the IHT derived from the CE in the tropics, especially in the TWP. We presented the vertical and the meridional extent of the CE. In Sect. 4, we discussed the difference between the CE derived in this study and the ITCZ determined and presented in previous studies. The consistency between the CE and measurements of other trace gases such as Ozone and methane from the previous were also discussed in Sect. 4. The discussion of the stability and uncertainty of this method were given in the Appendix.

2 Methods

2.1 GEOS-Chem setup

We used the global 3-D chemical transport model GEOS-Chem in version 13.0.0 (Bey et al., 2001) driven by meteorology input from the Goddard Earth Observing System (GEOS) of the NASA Global Modeling and Assimilation Office. GEOS-Chem Classic uses the TPCORE advection algorithm of (Lin and Rood, 1996) on the latitude-longitude grid of the archived GEOS meteorological data. The model was driven by the MERRA-2 reanalysis meteorological fields produced by the Global Modeling and Assimilation Office (GMAO) at the Goddard Space Flight Center. The basic setup of our model simulation was summarized in Table 1. We first used a coarse global simulation with a grid resolution of 2°x2.5° to determine the boundary conditions. Then, we performed nested simulations with the resolution of 0.5°x0.625° in the tropical zonal domain of 30° N to 30° S for the same period of the global simulation. The model runs used 72 vertical layers from the surface up to 10 hPa, and the output was saved for every day. We switched off the emissions of compounds except for the passive tracer and the chemistry in the model, so only the advection is in consideration.

2.2 Determination of the Chemical Equator (CE)

1) Description of how the CE is determined from the field of the passive trace

The passive tracer was released uniformly within the zonal range of 30° N - 90° N from the surface to 1 km from 2014 to 2019. Figure 1 shows the releasing area of the passive tracer. The uniform flux in the zonal range within the extra-tropics was to eliminate the regional dependency of the emission. After release, the tracer first accumulated in the north and then traveled

https://doi.org/10.5194/acp-2022-653
Preprint. Discussion started: 11 October 2022

Atmospheric Chemistry and Physics Discussions

to the south, with a stable north-south gradient pattern which was a result of air mass transport and atmospheric circulation. The time series of the tracer averaged zonally in six latitude bands are shown in Fig. 2a. After approximately one year of simulation, the linear growth rate is roughly equal in each latitude band. The meridional gradient of the passive tracer is similar to SF_6 shown in Fig. 2b. There is a clear increasing lag of 0.5-1.0 yr in the SH compared to the NH in SF_6. The similar time lag of the passive tracer that we used can also be seen in Fig. 2a, suggesting the possibility to use the passive tracer for the study of interhemispheric mixing.

To distinguish air mass transport from either one or the other hemisphere, the decomposition method is applied to the time series of the tracer, thus deriving the trend and the seasonality of the tracer. Since the variation around the trend does not vary with the level of the time series, an additive model of the decomposition is used:

$$y_t = T_t + S_t + R_t, \tag{1}$$

where y_t is the time series of the tracer, T_t is the trend component, S_t is the seasonal component, R_t is the residual component or noise. The subscript t denotes the time.

Figure 3 shows the decomposition of the time series of the passive tracer. Two grid boxes in the TWP are shown here for examples. One locates at 6.0° S, 127.5° E and the other locates at 6.0°N, 127.5°E, to represent the SH and NH respectively. The trend component in each grid box is a linear increase, as shown in Fig. 3a and Fig. 3b. The seasonal component of the grid box in the NH (as shown in Fig. 3a) varied from positive values to negative values year-round, which shows the higher concentration from the higher latitude bands and lower concentration from the lower latitude bands. For the grid box in the SH (shown in Fig. 3b), the seasonal component is positive only when a high concentration of the passive tracer is transported from the NH to this grid box. Otherwise, in other periods, approximately from March to November each year, the air mass from the south has a concentration value of zero, so the seasonal component is also around zero value.

After the decomposition, the trend of the tracer in each grid box can be given as $T_{t,i,j}$, where the subscript t, i, j refer to as the time, the longitude and attitude of the grid box, respectively. The trend in each grid box and each time step is meridional averaged in the longitude of range of -180° to 180° and zonally averaged in the latitude range of 30° S to 30° N:

$$\overline{T_t} = \overline{T_{t,i,j}},\ i\,\text{from}\,-180^\circ\,\text{to}\,180^\circ, j\,\text{from}\,30^\circ\,\text{S}\,\text{to}\,30^\circ\,\text{N}, \tag{2}$$

where $\overline{T_t}$ is the spatial average of the trend which is also the criterion of the CE at each time step t. Since the CE is defined in the tropics, the average range of the latitude (30° S to 30° N) is roughly representative of the location where the CE occurs. The location of the CE in each time step t , is given by $\overline{T_t}$, which is the spatial average at each time step of the trend, which indicates the tracer concentration on the CE:

$$CE_t = \left\{\text{where}: C_{i,j,t} = \overline{T_t}\right\}, \tag{3}$$

where $C_{i,j,t}$ is the tracer concentration in each grid box and each time step t . For example, if the tracer concentration in a grid box is higher than $\overline{T_t}$, this grid box is located on the NH, and vice versa for the SH.

2) Description of different experiments

https://doi.org/10.5194/acp-2022-653
Preprint. Discussion started: 11 October 2022


Atmospheric Chemistry and Physics Discussions

A series of tracer experiments were made to investigate the chemical equator and estimate the location of the CE by using the decomposition method as mentioned before. Two base experiments, Experiment 1 (E1) and Experiment 2 (E2), are carried out to study the air mass transport from both hemispheres by releasing the tracer either in the Northern or Southern extra-tropics latitude bands (see Fig. 1 and Table. 2). The tracer experiments follow the same format: the chemical inert tracers with infinite lifetime were released into the atmosphere with the constant flux of 1×10 kg/m2/s from the start to the end during each simulation. For the sake of simplicity and clarity, the methodology of determining the CE introduced before is described based on E1. In the base experiment E1, the tracer was released in the NH extra-tropics to determine the north boundary of the CE, which is abbreviated as CE-NH.

The setup of the E2 was the same as that of the E1, except that the passive tracer emission region was placed in the SH. With the same method introduced before but applied to the simulation results from the E2, we could obtain the south boundary of the CE, which for short is CE-SH. By comparing the results of the two base experiments E1 and E2, we obtain insights into the interhemispheric transport and answer an important question of whether the north and the south boundary of the CE coincide with each other when the passive tracer was released in different latitude bands coming from two different hemispheres. In the later article, the CE-NH is referred to as the north boundary calculated from the model results in E1, and the CE-SH is referred to as the south boundary calculated from the model results in E2. The region between these two boundary lines is where the interhemispheric mixing happens and is referred to as CE.

Apart from these two base experiments, there are other experiments Experiment 3 (E3) - Experiment 5 (E5) designed to investigate the stability of the method and to ensure that it is robust in different model settings. These experiments and the results are described in more detail in the Appendix, and the basic set-ups are summarized in Appendix Table 3. Releasing tracers on different altitude ranges does not affect the method. For example, the uniform release of the tracer between the surface and 10 km only affects the spin-up time of each experimental case, not the distribution of the tracer on the ground. This method can also be used to determine the location of CE in other years of interest like E5 (simulating from 2010 to 2015), which differs from the simulation starting time of E1-E4, indicating good repeatability of this method.

3 Results

3.1 The interhemispheric exchange indicated by the Chemical Equator

Figure 4 shows the daily locations of the CE-SH and CE-SH by colored scatters calculated from E1 (NH) and E2 (SH), respectively. Here we only present the CE in 2015 as an example. For other years (2016-2019) similar distribution of CE is given in the Supplement. In general, the method of using model simulation of the passive tracer can obtain the daily location of the CE of interest. Both CE-NH and CE-SH reach the south most position at the end of NH winter and the north most position at around 25° N in the end of NH summer. By comparing Fig. 4a and Fig. 4b, the CE-NH and CE-SH do not coincide with each other. In general, daily CE-SH is further south than the CE-NH. In February, CE-SH reaches around the south most position at 20° S in East Africa, the Indian Ocean, Central Pacific, and South America. This suggests that the south most position of

https://doi.org/10.5194/acp-2022-653
Preprint. Discussion started: 11 October 2022


Atmospheric Chemistry and Physics Discussions

interhemispheric exchange occurs on some days in late February. The north of the boundary at 20° S is dominated by the airmass transport from NH. In late August, except Africa, CE-NH in all other regions can reach the northernmost position of about 20° N, which indicated that the south of the boundary at 20° S is in the meteorological SH.

The seasonal average of CE from 2015 to 2019 is shown in Fig. 5. As the seasonal CE shown in Fig. 5, the interhemispheric exchange region between the NH and SH is a belt of meridional extent around the tropics. Since atmospheric transport is a continuous process, it is not a single boundary line separating the atmosphere and matter in the northern and southern hemispheres under objective conditions. The boundary is supposed to be a belt of longitudinal width in which air masses from the NH exchange and mix with those from the SH. In the following text, CE refers to this transition area between the north and the south boundary CE-NH and CE-SH, which are estimated by the method mentioned in Sec. 2 from E1 (NH) and E2 (SH), respectively.

As shown in Fig. 5a, from December to February, the CE lies on the south of the equator. After that, the CE moves north from March to August (shown in Fig.5b and 5c), crossing the equator to reach the geographical NH. The progressive domination of the tropical air masses from the SH in the NH spring and summer is characterized by the movement of the CE, in other words, the area down south of the boundary is located in the meteorological SH. In the NH autumn (Fig. 5d) and winter season (Fig. 5a), the air flows from the NH gradually strengthen, and the boundary moves southward , finally reaching its southernmost point in NH winter (shown in Fig. 5a). This suggests that the CE lags behind the ground position of the sun by about 3 months. This coincides with the time lag of the ITCZ.

To further study the migration of the atmospheric boundary between the two hemispheres and its correlation to the atmospheric circulation, we compare the patterns of the circulation over different regions together with the CE. Figure 7 shows the CE and zonally-averaged wind vectors in different regions defined as rectangular boxes within the tropical band between 30° S and 30° N (see Fig.6): Central & Eastern Pacific (CEP): 180° - 80° W; South America (SA): 80° W - 40° W; Atlantic (AT): 40° W - 15° W; Africa (AF): 15° W - 50° E; Indian Ocean (IO): 50° E - 100° W; Tropical Western Pacific (TWP): 100° E - 180°. The division of the regions is adapted from the definition of tropical regions in the literature of (Fueglistaler et al., 2004)

In general, the wind convergence zone is consistent with the latitude where the CE occurs, following a similar pattern, south of the equator in winter and north in summer, but there are regional differences. The wind convergence zone is consistent with the CE in the Central & Eastern Pacific and the Atlantic Ocean, as shown in Fig. 7 (CEP) and Fig. 7 (AT). Throughout the year, the north-easterly winds and the south-westerly winds meet, making a clear convergence zone near the equator from 0° to 10° N, and the CE lies in the confluence bands of the winds. The annual movement of the CE is relatively small in the Atlantic and Eastern Pacific, between 5° S and 10° N, indicating weaker seasonal shifts of the tropical circulation in those regions.

The seasonal movements of the CE are larger over the land sector, i.e. tropical South America and Africa, as shown in Fig. 7 (AF) and Fig. 7 (SA). In the NH winter, the CE-SH reaches its southernmost position at 15° S in South America in boreal winter from December to February. For the 10 m wind field in equatorial Africa and South America, the wind convergence zone does not coincide with the CE. In Africa, the confluence zone of north-easterly winds and south-westerly winds lies to the north of the CE. This suggests that air masses from the NH can continue to transport southward, with the area of interhemispheric exchange occurring further south to the convergence zone of the winds. For South America, we cannot see a significant

https://doi.org/10.5194/acp-2022-653
Preprint. Discussion started: 11 October 2022


Atmospheric Chemistry and Physics Discussions

wind field convergence zone in Fig. 7 (SA). The contrast between the north-easterly winds from the NH and the South-easterly winds from the SH is obvious, possibly due to the distribution of land and sea.

The circulation system in TWP and its interaction with the large-scale atmospheric circulation such as WPM and Hadley cell bring much complexity to the studies in this region. Over the TWP and the Indian Ocean, the annual movement of CE is larger compared to other ocean sectors, such as the Atlantic Ocean and Central & Eastern Pacific. From December to April, north-easterly winds deflect west after crossing the equator and converge with the south-easterly winds from the SH between about 0° and 5° S. From May to November, the convergence zone moves northward, while the south-easterly winds turn west after crossing the equator and the north-easterly winds converge north of the equator.

3.2 Vertical structure of the Chemical Equator

One advantage of our method of determining hemispheric boundaries is that the vertical structure of the boundaries can also be obtained from the model outputs. We first calculate CE at each level of the model output from the surface to the tropopause around 16 km. As fig. 8 shows, the CE-SH and CE-SH are more stable at lower levels than at higher ones. When the level goes up, it becomes hard to find an actual boundary between the two hemispheres due to the fast horizontal mixing by high-speed winds in the upper troposphere and lower stratosphere. So, we only take the level under 8 km into consideration, as Fig.8 shows. Here we only present the vertical structure in the CE in the TWP (100°E - 180°, 30°S - 30°N, see Fig. 6) as a focus. For other regions specified in Fig. 6, the vertical results of the CE are shown in the Supplement.

In general, the vertical sections of the hemispheric boundary of the atmosphere differ with seasons. From January to March, CE tends to tilt north. During these three months, air masses from the NH that are less than 2 km move south of the geographic equator, while the area above is occupied by air masses from the SH. From April, the oblique structure became less pronounced and the CE began to be vertical to the ground. From June to October, CE begins to tilt south. It should be noted that CE-NH slopes southward from the ground up, while CE-SH slopes from the ground to 2 km and is relatively vertical to the ground. This could indicate that the circulation system from the SH near the ground does not move further north in the summer, but stays near the equator, forming a broader north-south mixing region in the boundary layer. In November, CE resumed vertical to ground level. In December, CE showed a slightly sloping trend to the north. Similar to the actual emission level of the atmospheric component, the emission level of the passive tracer is from the ground to 1 km as mentioned in the model setups Sect. 2. When there is an emission source of the species in the bottom layer, the movement speed of CE decreases with the increase of the level.

3.3 The Chemical Equator versus the tropical rain belt in the TWP region

The rain belt is usually regarded as an indicator of the equatorial convergence zone and thus the boundary for interhemispheric exchange. However, the rain belt in the TWP region is relatively complex due to the convergence of the commonly defined ITCZ and its annual movement. Here, we compare the rain rate with the CE in the TWP region: Fig. 9 shows the zonally

https://doi.org/10.5194/acp-2022-653
Preprint. Discussion started: 11 October 2022


Atmospheric Chemistry and Physics Discussions

averaged rain rate averaged from 2015 to 2019 and the results of the E1 and E2 simulation as a rate of occurrence, i.e., the number of days that the CE occurs at each latitude as a percentage of the total appearance:

$$f_i = \frac{d_i}{\sum d_i}, \tag{4}$$

where f_i is the rate, i denotes the latitude, d_i is the number of days that the CE-SH / CE-NH locate in the latitude i . Because the CE-SH / CE-SH can be given daily, the higher the rate, the higher the latitude at which CE occurs most frequently during the month, and indicates the zone where the atmospheric exchange between the NH and SH.

In general, as shown in Fig. 9 the latitude range of CE occurrences is more concentrated within a month, relative to the location of rain bands. From May to October, in the summer and autumn, the southern peak and the northern peak of the rain belt coincide at the southern and northern boundaries of the hemispheric exchange, respectively, indicating that the location of the north-south rain belt during this time is related to the circulation system exchanged between the two hemispheres.

It is worth noting that both CE-NH and CE-SH tend to be at the southern peak of the rain band in the winter and early spring, from December to March. During these months, the northern rain band is outside the range where CE appears. The northern branch of the rain belt is not associated with the interhemispheric exchange. This suggests that the northern branch of the rain belt should be related to the circulation system of the NH at around 5-10° N rather than the system of interhemispheric exchange.

The seasonal cycle of the CE in two cases of NH and SH with the rain rate in the TWP region is shown in Fig. 10. The meridional extent of the transition area between the NH and SH varies with season. Similar to the monthly results shown in Fig. 9, the interhemispheric region is relatively broader in boreal summer than in other seasons. During NH winter (December–January) and spring (March-May), the transition area is narrow, and the northern part of the rain belt around 10° N is located north of the CE, while the southern part is included. This indicates, that the cause of the precipitation in the northern part of the TWP region is not the convergence of the equatorial flow from the NH and SH, but dependent on regional circulation within the NH. During NH summer (June-August) the meridional extent of the CE belt is the largest, including the northern rain belt. During NH autumn (September-November), the northern border began to retreat southward, and the transition area narrowed again and consistent with the two rain belts in the NH and SH.

4 Discussions

In general, the CE is consistent with the pattern of the tropical rain belt according to the tropical rain belt shown in the previous studies (e.g., Adam et al., 2016; Schneider et al., 2014). Since the location of CE indicates where atmospheres from the NH and SH meet, the airflow meets and causes precipitation to form in a manner consistent with the location of tropical rain belts occurring in yearly respect. The seasonal migration of CE is more stable across the oceans than lands , specifically in the East Pacific and the Atlantic. In these two regions, previous studies defined the convergence zone via the tropical rain belt (Gu2), low cloud-top temperature (Waliser and Gautier, 1993), and the magnitude of the horizontal gradient (Berry and Reeder, 2014)

https://doi.org/10.5194/acp-2022-653
Preprint. Discussion started: 11 October 2022


Atmospheric Chemistry and Physics Discussions

are consistent with the CE.

The atmospheric circulation system is more complicated on the continents compared to the ocean. It is modulated by several regional features such as local atmospheric jets and waves, proximity to the oceans, terrain-induced convective systems, moisture recycling, and spatiotemporal variability of land cover and albedo, so the location of the tropical rain belt becomes diffuse and does not coincide with the atmospheric boundary of the hemispheres (e.g., Arraut et al., 2012; Dez; Magee and Verdon-Kidd, 2018). As mentioned in Sect. 3.3, the meridional extent above the continents South America and tropical America is larger than the near ocean sectors. Considering the land-sea distribution contrast and the complexity of the circulation system over the tropical continent, we investigated the atmospheric boundary between the two hemispheres over the continents, more studies are needed on the regional circulation in tropical continental regions.

Previous studies (Hamilton et al., 2008; Petersen et al., 2010; Zhou et al., 2018; Müller, 2020) based on trace gas observations by aircraft, ozone soundings, and Fourier transform infrared (FTIR) spectrometers in the tropical regions were aimed to have a better understanding of the tropical dynamics. During NH winter, the high concentration of the pollution tracers such as CO and Ozone from Southeastern Asia by large-scale circulation tends to be modulated by the migration of the ITCZ (Hamilton et al., 2008; Müller, 2020). This phenomenon was also captured by our method, as shown in Fig. 10 (December-January). The region on the north of the CE-NH which is at around 5° S is at meteorological NH, indicating that the airmass origins are from NH. The FTIR measurements of methane and CO in the tropical sites, Suriname (5.8° N, 55.2° W) also suggested that the seasonal variation of the CH_4 was highly related to the interhemispheric transport (Petersen et al., 2010). In Reunion Island (21° S, 55° E), the high spike of CH_4 coming from the NH was captured by the FTIR measurements in the local summer (December-February) (Zhou et al., 2018). As shown in Fig. 4, the CE locates around 20° S during this period, which is consistent with the observation of the CH_4. The consistent results of the trace gases and our method of CE in the tropical sites suggest a potential that we can use CE as a good and objective tool to determine the airmass origin and understand the tropical dynamics.

5 Conclusions

We introduced a new method to investigate interhemispheric air mass transport in the tropical region by passive tracer simulations with GEOS-Chem. The so-called CE indicates the region where air masses exchange between the two hemispheres occurs.

The daily CE showed reasonable agreement with the pattern of the tropical rain belt. By comparing the CE with the wind field in different regions, we find that the confluence of the equatorial flow is consistent with CE where interhemispheric mixing occurs in the Central Eastern Pacific and the Atlantic Ocean. In Africa, where the zone of the confluence is in the north of the CE, which is needed to be further investigated. The vertical extent of the CE varied with the seasons. It slopes northward from the ground to the upper air in winter, is nearly perpendicular to the ground in the spring, and slopes southward in the summer. The tilt of the CE diminishes in the fall and returns to a pattern that is vertical to the ground. We further focus on the

https://doi.org/10.5194/acp-2022-653
Preprint. Discussion started: 11 October 2022

Atmospheric Chemistry and Physics Discussions

relationship between the CE and the tropical rain belt in the TWP region. The north-south migration of the CE is consistent with the maximum rain rate during a year.

Considering the air mass exchange is a continuous process, we made a simulation case with the release of the passive tracer in the SH. The transition area of the interhemispheric mixing is given. Its extent varies with season and region. Two cases set in the two symmetry fluxes region in the NH and SH help to obtain a complete pattern of the interhemispheric mixing. This mixing process happens in a transition area, with a continuous gradient rather than a single border separating the atmosphere in the NH and SH. From this transition area, we find that the northern part of the precipitation band in the TWP in winter is more likely caused by the regional circulation rather than the convergence of the equatorial flow from the NH and SH. By combining the CE determined from the southern and NH emission zones, we thus get further insights into interhemispheric exchange in the TWP region.

The simulation results will be complemented by observational data in the future. It can be used to categorize the trace gases in the TWP region and supplement the source and sink analysis of trace gases in this region. Since the TWP is an area of the active troposphere to stratosphere exchange, the seasonal and in particular vertical characteristics of the CE will be valuable for studies of troposphere / stratospheric exchange.

Appendix A: appendix

E3 to E5 are three supplement case studies with different emission regions and vertical layers compared to E1 and E2; the setting of the simulations are shown in Table A. These cases are aimed to test the stability of our method to determine the CE. It should be noted that the north-south gradient of this passive tracer is the preliminary condition of the method and the definition of the CE. So, the emissions of the tracer must exist continuously in one hemisphere to create and maintain this gradient, rather than an equilibrated atmosphere.

Code availability. The GEOS-Chem model code used in this analysis is downloaded from the GEOS-Chem "Science" Codebase repository: https://github.com/geoschem/geos-chem. The code for calculating the CE is available at https://github.com/XiaoyuSun-n/Chemical-Equator.

Data availability. The Meteorology input data used in this analysis are availble at http://geoschemdata.wustl.edu/. The model output, the reults of the CE are available at: https://doi.org/10.5281/zenodo.7018391 (Sun et al., 2022).

Author contributions. XS and MP designed the study. XS conducted the model simulation and made the analysis. XS wrote the manuscript, with contributions from all coauthors.

https://doi.org/10.5194/acp-2022-653
Preprint. Discussion started: 11 October 2022

Atmospheric Chemistry and Physics Discussions

Competing interests. The co-author Mathias Palm is a co-editor of ACP. Besides that, the contact author has declared that they don't have any other competing interests.

Acknowledgements. The authours acknowledge the GEOS-Chem Support Team at Harvard University and Dalhousie University for their effort. We also thank the support team in geos-chem github (issues). They gave us precious answers and resolved our doubts about GEOS-Chem models. This work has been supported by the BMBF (German Ministry of Research and Education) in the project ROMIC-II subproject TroStra (01LG1904A). We thank the AWI Potsdam and the Impres GmbH, Bremen, for logistical and technical support in Palau. We also thank the Coral Research foundation (CRRF) and the PCC Palau for support in conducting the measurements. We also thank the Senate of Bremen for partial support.

https://doi.org/10.5194/acp-2022-653
Preprint. Discussion started: 11 October 2022

Atmospheric Chemistry and Physics Discussions

References

Adam, O., Bischoff, T., and Schneider, T.: Seasonal and Interannual Variations of the Energy Flux Equator and ITCZ. Part I: Zonally Averaged ITCZ Position, J. Climate, 29, 3219 – 3230, https://doi.org/10.1175/JCLI-D-15-0512.1, 2016.

Arraut, J. M., Nobre, C., Barbosa, H. M. J., Obregon, G., and Marengo, J.: Aerial Rivers and Lakes: Looking at Large-Scale Moisture Transport and Its Relation to Amazonia and to Subtropical Rainfall in South America, J. Climate, 25, 543 – 556, https://doi.org/10.1175/2011JCLI4189.1, 2012.

Berry, G. and Reeder, M. J.: Objective Identification of the Intertropical Convergence Zone: Climatology and Trends from the ERA-Interim, J. Climate, 27, 1894 – 1909, https://doi.org/10.1175/JCLI-D-13-00339.1, 2014.

Bey, I., Jacob, D. J., Yantosca, R. M., Logan, J. A., Field, B. D., Fiore, A. M., Li, Q., Liu, H. Y., Mickley, L. J., and Schultz, M. G.: Global modeling of tropospheric chemistry with assimilated meteorology: Model description and evaluation, J. Geophys. Res., 106, 23 073–23 095, https://doi.org/https://doi.org/10.1029/2001JD000807, 2001.

Fueglistaler, S., Wernli, H., and Peter, T.: Tropical troposphere-to-stratosphere transport inferred from trajectory calculations, J. Geophys. Res., 109, https://doi.org/https://doi.org/10.1029/2003JD004069, 2004.

Geller, L. S., Elkins, J. W., Lobert, J. M., Clarke, A. D., Hurst, D. F., Butler, J. H., and Myers, R. C.: Tropospheric SF6: Observed latitudinal distribution and trends, derived emissions and interhemispheric exchange time, Geophys. Res. Lett., 24, 675–678, https://doi.org/https://doi.org/10.1029/97GL00523, 1997.

Hall, B. D., Dutton, G. S., Mondeel, D. J., Nance, J. D., Rigby, M., Butler, J. H., Moore, F. L., Hurst, D. F., and Elkins, J. W.: Improving measurements of SF_6 for the study of atmospheric transport and emissions, Atmos. Meas. Tech., 4, 2441–2451, https://doi.org/10.5194/amt-4-2441-2011, 2011.

Hamilton, J. F., Allen, G., Watson, N. M., Lee, J. D., Saxton, J. E., Lewis, A. C., Vaughan, G., Bower, K. N., Flynn, M. J., Crosier, J., Carver, G. D., Harris, N. R. P., Parker, R. J., Remedios, J. J., and Richards, N. A. D.: Observations of an atmospheric chemical equator and its implications for the tropical warm pool region, J. Geophys. Res., 113, https://doi.org/https://doi.org/10.1029/2008JD009940, 2008.

Krüger, K., Tegtmeier, S., and Rex, M.: Long-term climatology of air mass transport through the Tropical Tropopause Layer (TTL) during NH winter, Atmos. Chem. Phys., 8, 813–823, https://doi.org/10.5194/acp-8-813-2008, 2008.

Lin, S.-J. and Rood, R. B.: Multidimensional Flux-Form Semi-Lagrangian Transport Schemes, Mon. Weather. Rev., 124, 2046 – 2070, https://doi.org/10.1175/1520-0493(1996)124<2046:MFFSLT>2.0.CO;2, 1996.

Magee, A. D. and Verdon-Kidd, D. C.: On the relationship between Indian Ocean sea surface temperature variability and tropical cyclogenesis in the southwest Pacific, Int. J. Climatol., 38, e774–e795, https://doi.org/https://doi.org/10.1002/joc.5406, 2018.

Morris, R. A., Miller, T. M., Viggiano, A. A., Paulson, J. F., Solomon, S., and Reid, G.: Effects of electron and ion reactions on atmospheric lifetimes of fully fluorinated compounds, J. Geophys. Res., 100, 1287–1294, https://doi.org/https://doi.org/10.1029/94JD02399, 1995.

Müller, K.: Characterization of Ozone and the Oxidizing Capacity of the Tropical West Pacific Troposphere, Ph.D. thesis, Fachbereich Physik und Elektrotechnik der Universität Bremen, Germany, 2020.

Newell, R. E. and Gould-Stewart, S.: A Stratospheric Fountain?, J. Atmos. Sci., 38, 2789 – 2796, https://doi.org/10.1175/1520-0469(1981)038<2789:ASF>2.0.CO;2, 1981.

https://doi.org/10.5194/acp-2022-653
Preprint. Discussion started: 11 October 2022

Atmospheric Chemistry and Physics Discussions

Nicholson, S. E.: A revised picture of the structure of the "monsoon" and land ITCZ over West Africa, Clim. Dynam., 32, 1155–1171, https://doi.org/10.1007/s00382-008-0514-3, 2009.

Nicholson, S. E.: The ITCZ and the Seasonal Cycle over Equatorial Africa, B. Am. Meteor. Soc., 99, 337 – 348, https://doi.org/10.1175/BAMS-D-16-0287.1, 2018.

Petersen, A. K., Warneke, T., Frankenberg, C., Bergamaschi, P., Gerbig, C., Notholt, J., Buchwitz, M., Schneising, O., and Schrems, O.: First ground-based FTIR observations of methane in the inner tropics over several years, Atmos. Chem. Phys., 10, 7231–7239, https://doi.org/10.5194/acp-10-7231-2010, 2010.

Ramage, C. S.: ROLE OF A TROPICAL "MARITIME CONTINENT" IN THE ATMOSPHERIC CIRCULATION, Mon. Weather. Rev., 96, 365 – 370, https://doi.org/10.1175/1520-0493(1968)096<0365:ROATMC>2.0.CO;2, 1968.

Ravishankara, A. R., Solomon, S., Turnipseed, A. A., and Warren, R. F.: Atmospheric Lifetimes of Long-Lived Halogenated Species, Science, 259, 194–199, https://doi.org/10.1126/science.259.5092.194, 1993.

Ray, E. A., Moore, F. L., Elkins, J. W., Rosenlof, K. H., Laube, J. C., Röckmann, T., Marsh, D. R., and Andrews, A. E.: Quantification of the SF6 lifetime based on mesospheric loss measured in the stratospheric polar vortex, J. Geophys. Res., 122, 4626–4638, https://doi.org/https://doi.org/10.1002/2016JD026198, 2017.

Rex, M., Wohltmann, I., Ridder, T., Lehmann, R., Rosenlof, K., Wennberg, P., Weisenstein, D., Notholt, J., Krüger, K., Mohr, V., and Tegtmeier, S.: A tropical West Pacific OH minimum and implications for stratospheric composition, Atmos. Chem. Phys., 14, 4827–4841, https://doi.org/10.5194/acp-14-4827-2014, 2014.

Rigby, M., Mühle, J., Miller, B. R., Prinn, R. G., Krummel, P. B., Steele, L. P., Fraser, P. J., Salameh, P. K., Harth, C. M., Weiss, R. F., Greally, B. R., O'Doherty, S., Simmonds, P. G., Vollmer, M. K., Reimann, S., Kim, J., Kim, K.-R., Wang, H. J., Olivier, J. G. J., Dlugokencky, E. J., Dutton, G. S., Hall, B. D., and Elkins, J. W.: History of atmospheric SF_6 from 1973 to 2008, Atmos. Chem. Phys., 10, 10 305–10 320, https://doi.org/10.5194/acp-10-10305-2010, 2010.

Schneider, T., Bischoff, T., and Haug, G. H.: Migrations and dynamics of the intertropical convergence zone, Nature, 513, 45–53, https://doi.org/10.1038/nature13636, 2014.

Smith, I. N., Moise, A. F., and Colman, R. A.: Large-scale circulation features in the tropical western Pacific and their representation in climate models, J. Geophys. Res., 117, https://doi.org/https://doi.org/10.1029/2011JD016667, 2012.

Stehr, J. W., Ball, W. P., Dickerson, R. R., Doddridge, B. G., Piety, C. A., and Johnson, J. E.: Latitudinal gradients in O3 and CO during INDOEX 1999, J. Geophys. Res., 107, INX2 15–1–INX2 15–8, https://doi.org/https://doi.org/10.1029/2001JD000446, 2002.

Waliser, D. E. and Gautier, C.: A Satellite-derived Climatology of the ITCZ, J. Climate, 6, 2162 – 2174, https://doi.org/10.1175/1520-0442(1993)006<2162:ASDCOT>2.0.CO;2, 1993.

Wang, C. and Magnusdottir, G.: The ITCZ in the Central and Eastern Pacific on Synoptic Time Scales, Mon. Weather. Rev., 134, 1405 – 1421, https://doi.org/10.1175/MWR3130.1, 2006.

Waugh, D. W., Crotwell, A. M., Dlugokencky, E. J., Dutton, G. S., Elkins, J. W., Hall, B. D., Hintsa, E. J., Hurst, D. F., Montzka, S. A., Mondeel, D. J., Moore, F. L., Nance, J. D., Ray, E. A., Steenrod, S. D., Strahan, S. E., and Sweeney, C.: Tropospheric SF6: Age of air from the Northern Hemisphere midlatitude surface, J. Geophys. Res., 118, 11,429–11,441, https://doi.org/https://doi.org/10.1002/jgrd.50848, 2013.

Williams, J., Fischer, H., Wong, S., Crutzen, P. J., Scheele, M. P., and Lelieveld, J.: Near equatorial CO and O3 profiles over the Indian Ocean during the winter monsoon: High O3 levels in the middle troposphere and interhemispheric exchange, J. Geophys. Res., 107, INX2 6–1–INX2 6–13, https://doi.org/https://doi.org/10.1029/2001JD001126, 2002.

https://doi.org/10.5194/acp-2022-653
Preprint. Discussion started: 11 October 2022

Yang, H., Waugh, D. W., Orbe, C., Patra, P. K., Jöckel, P., Lamarque, J.-F., Tilmes, S., Kinnison, D., Elkins, J. W., and Dlugokencky, E. J.: Evaluating Simulations of Interhemispheric Transport: Interhemispheric Exchange Time Versus SF6 Age, Geophys. Res. Lett., 46, 1113–1120, https://doi.org/https://doi.org/10.1029/2018GL080960, 2019.

Zhou, M., Langerock, B., Vigouroux, C., Sha, M. K., Ramonet, M., Delmotte, M., Mahieu, E., Bader, W., Hermans, C., Kumps, N., Metzger, J.-M., Duflot, V., Wang, Z., Palm, M., and De Mazière, M.: Atmospheric CO and CH_4 time series and seasonal variations on Reunion Island from ground-based in situ and FTIR (NDACC and TCCON) measurements, Atmos. Chem. Phys., 18, 13 881–13 901, https://doi.org/10.5194/acp-18-13881-2018, 2018.

https://doi.org/10.5194/acp-2022-653
Preprint. Discussion started: 11 October 2022

Atmospheric Chemistry and Physics Discussions

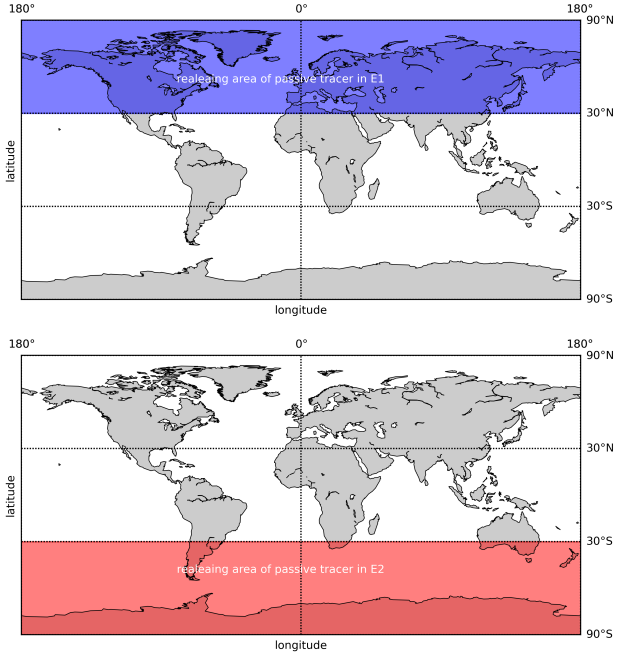

Figure 1. The releasing area of passive tracer E1 (shown by shaded blue region) and E2 (shown by shaded red region)

https://doi.org/10.5194/acp-2022-653
Preprint. Discussion started: 11 October 2022

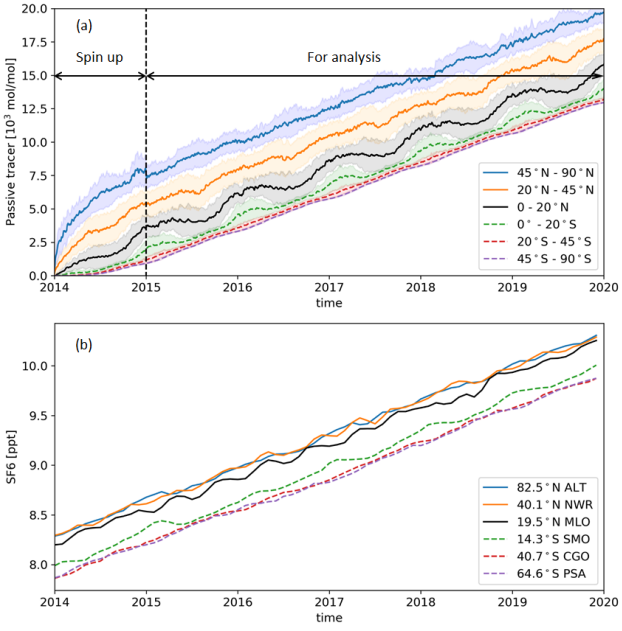

Figure 2. Comparison of the passive tracer and SF_6. (a) Zonally averaged amount of the passive tracer from GEOS-Chem simulations from 2014-2019 as a function of time for three northern (solid lines) and three southern (dashed lines) latitude ranges (0°-20°, 20°-45°, 45°-90°). The value of the concentration of the passive tracer is not meaningful to the studies since we only take into account the relative higher or lower amount of the tracer. 1-σ of the passive tracer of each latitude band is shown in shaded color. (b) SF_6 monthly means from Combined Sulfur hexafluoride data from the NOAA/ESRL Global Monitoring Division at six stations corresponding to the latitude bands in Fig.1a (ALT: Alert (82.5° N, 62.3° W), NWR: Niwot Ridge (40.1° N, 105.6° W), MLO: Mauna Loa (19.5° N, 155.6° W), SMO: Cape Matatula (14.3° S, 170.6° W), CGO: Cape Grim (40.7° S, 144.8° E), PSA: Palmer Station (64.6° S, 64.0° W)).

https://doi.org/10.5194/acp-2022-653
Preprint. Discussion started: 11 October 2022

Atmospheric Chemistry and Physics Discussions

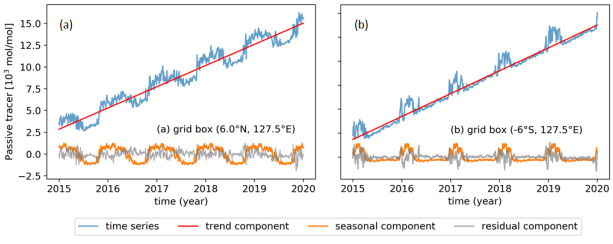

Figure 3. Time series of the passive tracer (blue line), trend component (red line), seasonal component (orange line), and residual component (grey line) of the passive tracer as a function of time (2015-2019) in two example grid boxes (a) [6.0° S, 127.5° E] and (b) [6.0° N, 127.5° E].

https://doi.org/10.5194/acp-2022-653
Preprint. Discussion started: 11 October 2022

Atmospheric Chemistry and Physics Discussions

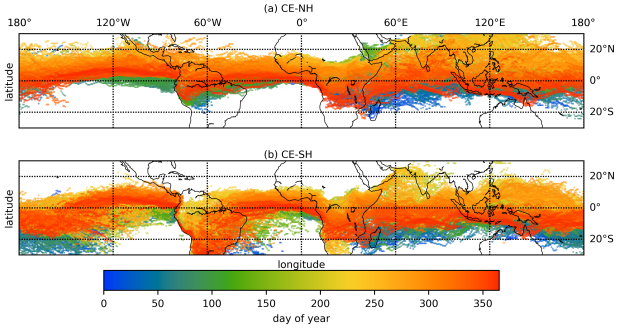

Figure 4. Daily CE-NH and CE-SH calculated from model simulations of (a) E1 (tracer released in NH) and (b) E2 (tracer released in SH) in 2015; the color shows the day of the year.

https://doi.org/10.5194/acp-2022-653
Preprint. Discussion started: 11 October 2022

Atmospheric Chemistry and Physics Discussions

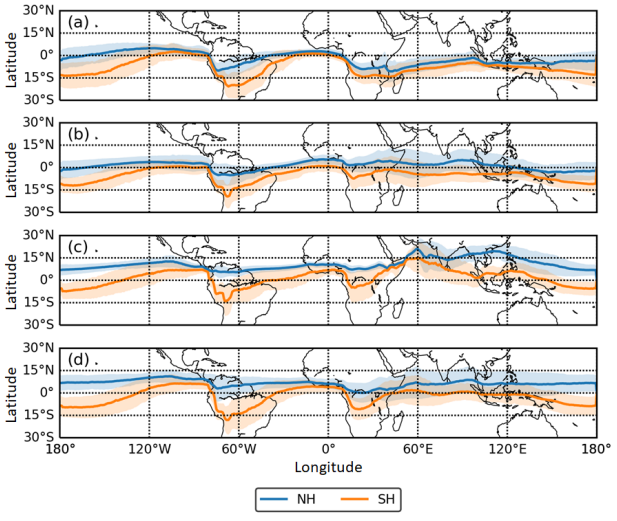

Figure 5. 5-year (2015-2019) averaged seasonal location of CE. (a) December, January, and February. (b) March, April, and May. (c) June, July, and August. (d) September, October, and November. 1-σ of the CE of each season is shown in shaded color.

https://doi.org/10.5194/acp-2022-653
Preprint. Discussion started: 11 October 2022

Atmospheric Chemistry and Physics Discussions

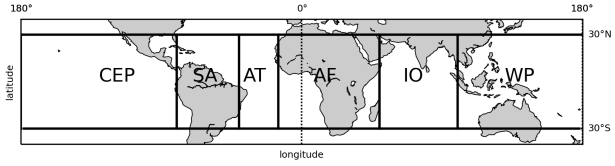

Figure 6. Definition of geographic regions in this study. Central East Pacific (CEP): (180°, 80°W); South America (SA): (80°W, 40°W); Atlantic (AT): (40°W, 15°W); Africa (AF): (15°W, 50°E),; Indian Ocean (IO): (50°E, 100°E); Tropical West Pacific (TWP): (100°E, 180°); all these regions are with the same latitude range: 30°S - 30°N.

https://doi.org/10.5194/acp-2022-653
Preprint. Discussion started: 11 October 2022

Atmospheric Chemistry and Physics Discussions

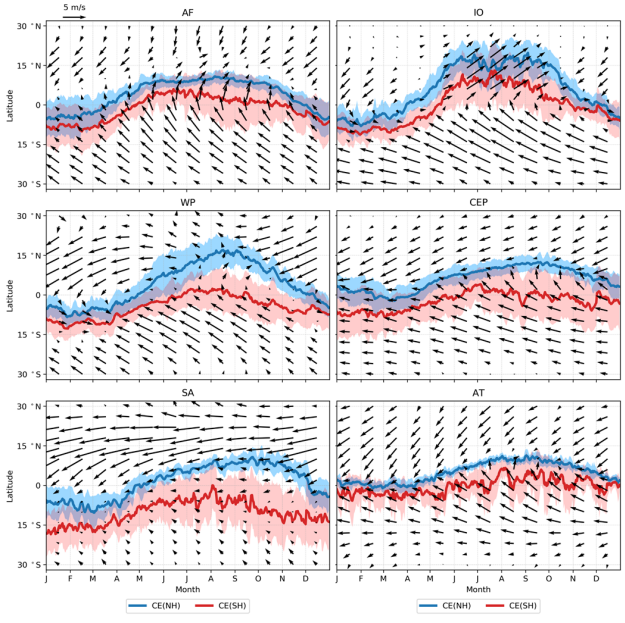

Figure 7. Monthly averaged wind vectors (black arrows) and annual movement of the daily CE. The blue lines show the NH boundary and the red lines show the SH boundary. The wind data are the 10-m winds from the ERA5 reanalysis data (Hersbach et al., 2020) averaged from 2015 to 2019. Both the CE and the wind field are space averaged zonally in eight different regions such as Africa (AF) and IO (Indian Ocean). The abbreviations and definition of the region on the top of each subplot are according to Fig. 6. 1-σ of the CE is shown in shaded color.

https://doi.org/10.5194/acp-2022-653
Preprint. Discussion started: 11 October 2022

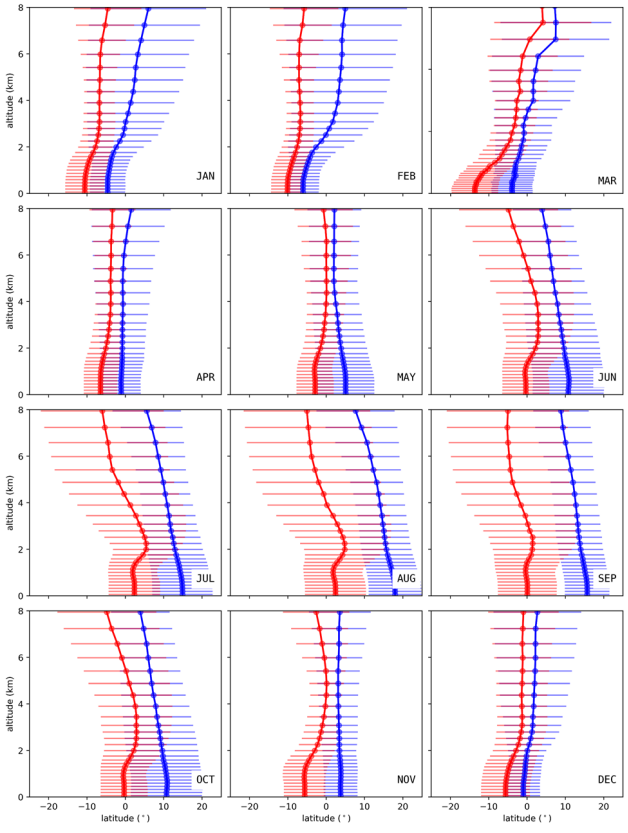

Figure 8. Monthly averaged (2015-2019) CE by altitude. The CE-NH / CE-SH are zonally (100° E-180°) averaged over the TWP region see Fig. 6. The blue lines show the CE-NH and the red lines show the CE-SH. Only CE-NH / CE-SH below 8 km are shown here because of the large uncertainty in the higher model level. 1-σ of the CE-NH and CE-SH are given in the plots.

https://doi.org/10.5194/acp-2022-653
Preprint. Discussion started: 11 October 2022

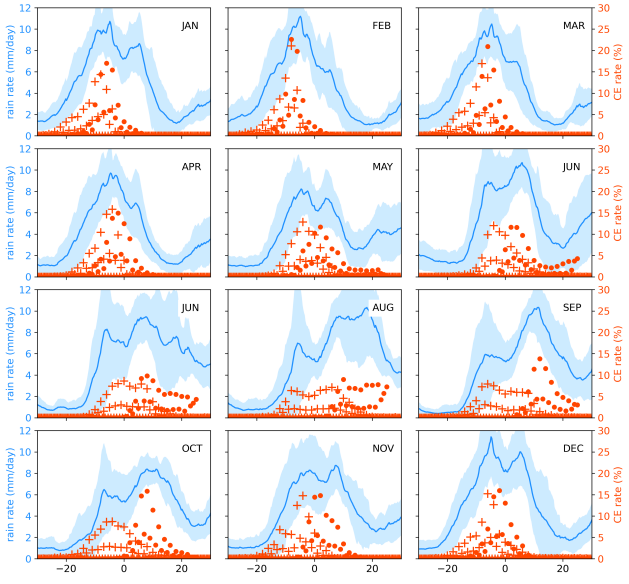

Figure 9. 5-year averaged (2015-2019) monthly rate of the CE-NH / CE-SH (red) with the rain rate (blue) from TRMM (Tropical Rainfall Measuring Mission) products 3B43 (monthly) (Huffman et al., 2007) as a function of latitude averaged over the West Pacific region (same definition as Fig. 6). The CE-SH is marked as '+' and the CE-NH is marked as dot. The data in this plot are also zonally averaged in the TWP region specified in Fig. 5.

https://doi.org/10.5194/acp-2022-653
Preprint. Discussion started: 11 October 2022

Atmospheric Chemistry and Physics Discussions

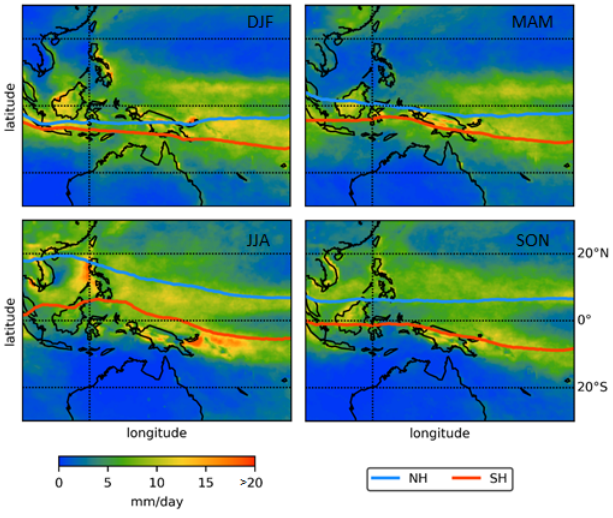

Figure 10. Seasonal rain rate (color scale) from TRMM (same dataset as Fig. 9) in the TWP region with the blue line showing CE-NH and the red line showing CE-SH.

https://doi.org/10.5194/acp-2022-653
Preprint. Discussion started: 11 October 2022

Atmospheric Chemistry and Physics Discussions

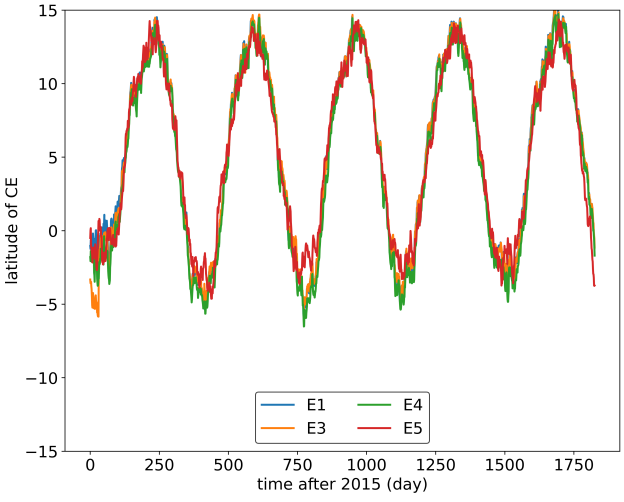

Figure A1. Comparison of the CE-NH in the basic experiment E1 with experiments E3 to E5. 5-year (2015-2019) zonally averaged daily latitude of all CE-NH.

https://doi.org/10.5194/acp-2022-653
Preprint. Discussion started: 11 October 2022

Atmospheric Chemistry and Physics Discussions

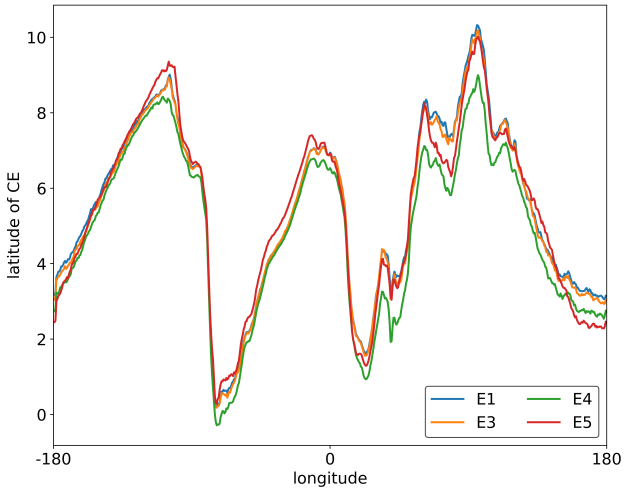

Figure A2. Comparison of the CE-NH in the basic experiment E1 with experiments E3 to E5. 5-year (2015-2019 or 2011-2015) daily latitude of all CE relative to longitude.

https://doi.org/10.5194/acp-2022-653
Preprint. Discussion started: 11 October 2022

Atmospheric Chemistry and Physics Discussions

Table 1. The settings of GEOS-Chem v13.0.0 used in this study

Resolution	2° x 2.5° (Global simulation), 0.5° x 0.625° (Nested simulation), 72 levels
Simulated species	Passive tracer
Global inventory	none
Meteorology field	MERRA-2
Tracer lifetime	Infinite
Tracer emission	Constantly released after starting the simulation
Tracer chemical process	none
Transport / Convection timestep	600 s

https://doi.org/10.5194/acp-2022-653
Preprint. Discussion started: 11 October 2022

Atmospheric Chemistry and Physics Discussions

Table 2. The settings of two base experiments

Experiment	Release area	Release layer	Simulated time
E1 (NH)	30° N - 90° N, zonally	Surface - 1 km	years (2014 - 2019)
E2 (SH)	30° S - 90° S, zonally		

https://doi.org/10.5194/acp-2022-653
Preprint. Discussion started: 11 October 2022

Atmospheric Chemistry and Physics Discussions

Table A1. The settings for experiment E3 to experiment E5

Experiment	Release area	Release layer	Simulated time
E3	30° N - 70° N, -180° - 180°	Surface - 1 km	5 years (2014 - 2019)
E4	30° N - 90° N, -180° - 180°	Surface - 10 km	5 years (2014 - 2019)
E5	30° N - 90° N, -180° - 180°	Surface - 1 km	5 years (2010 - 2015)